GEOMORPHOLOGY

Erosion by an Alpine glacier

Frédéric Herman,[1]* Olivier Beyssac,[2] Mattia Brughelli,[1] Stuart N. Lane,[1] Sébastien Leprince,[3] Thierry Adatte,[4] Jiao Y. Y. Lin,[5] Jean-Philippe Avouac,[3] Simon C. Cox[6]

Assessing the impact of glaciation on Earth's surface requires understanding glacial erosion processes. Developing erosion theories is challenging because of the complex nature of the erosion processes and the difficulty of examining the ice/bedrock interface of contemporary glaciers. We demonstrate that the glacial erosion rate is proportional to the ice-sliding velocity squared, by quantifying spatial variations in ice-sliding velocity and the erosion rate of a fast-flowing Alpine glacier. The nonlinear behavior implies a high erosion sensitivity to small variations in topographic slope and precipitation. A nonlinear rate law suggests that abrasion may dominate over other erosion processes in fast-flowing glaciers. It may also explain the wide range of observed glacial erosion rates and, in part, the impact of glaciation on mountainous landscapes during the past few million years.

Glaciers and icecaps played a major role in shaping the morphology of mid- to high-latitude mountain ranges during the Quaternary period, spanning the past 2.6 million years of Earth's history. Observations suggest that they have also played a fundamental role in the evolution of Earth's climate through a system of positive feedbacks that involves climate, tectonics, and erosion (*1*–*4*). Glaciers erode their underlying bedrock mainly through abrasion and quarrying, which theories predict to be proportional to ice-sliding velocity raised to some power (*5*–*7*). Numerical models reproduce typical glacial landscape features, such as U-shaped valleys (*3*, *8*), hanging valleys (*9*, *10*), glacial cirques (*10*, *11*), or fjords (*12*, *13*), by implementing these relationships. Despite great advances in the sophistication of these models through the inclusion of high-order ice dynamics (*10*), subglacial hydrology (*10*, *11*, *13*–*15*), or thermodynamics of water flow (*14*, *16*), they also include poorly constrained parameters. Erosion laws' proportionality constants and velocity exponents are particularly uncertain (*5*–*8*, *11*, *13*).

Estimates of glacial erosion rates ranging from annual to million-year time scales come from monitoring the sediment yield from glacial streams (*17*–*21*) and using geochronometric methods (*4*, *18*), respectively. Despite providing key information about the pace at which glaciers may shape mountainous landscapes, these studies have not established an accurate law for glacial erosion. Furthermore, estimates of glacial erosion rates vary by four orders of magnitude from polar to temperate regions on Earth (*4*, *17*, *18*). Existing theories do not reproduce such variations. Therefore, our current understanding of the link between climate and glacial erosion suffers from poor constraints on what controls spatial and temporal erosion variability in response to global changes in precipitation and temperature.

We designed this study to specifically constrain how glacial erosion relates to ice-sliding velocity. We simultaneously quantified erosion rates and sliding velocity during a 5-month period, from November 2013 to April 2014, over the entire Franz Josef Glacier, New Zealand. This glacier exhibits surface velocities that are largely dominated by high sliding velocities on the bedrock (*22*), up to about 3 m/day. We measured these high velocities accurately from remote sensing and expected to find large erosion rates. The analysis of continuous suspended sediment load indicated very high erosion rates (about 10 mm/year), whereas glacial sediment production remained lower than the transport capacity of the glacial system (*23*). We also found that the glacial sediments come predominantly from under the glacier, based on the mineralogy, fossil organic carbon, and the very low fraction of modern organic carbon found in the glacial stream (*23*). These observations imply that sediments collected at the glacier front can be used to constrain the glacial erosion law.

We introduce here a method to measure surface displacement in three dimensions at a 1-m ground resolution and centimetric accuracy, using DigitalGlobe Worldview stereopair images (*23*). The results confirm fast velocities for most parts of the glacier (Fig. 1) dominated by sliding (*22*, *23*). In addition, we observed similar velocity patterns during the austral summers 2012–2013 and 2013–2014, indicating steady spatial patterns of sliding. Extremely high snow accumulation rates of 4 to 8 m/year (water equivalent) (*24*) and steep topography account for such high velocities (*22*).

We exploited the geology of the Southern Alps of New Zealand to determine how erosion varies spatially. This small mountain range resulted from the continental collision between the Australian and Pacific Plates, along a major plate boundary named the Alpine Fault (*25*), which led to a sharp metamorphic gradient within a 15-km distance (Fig. 2). Rocks adjacent to the Alpine Fault have experienced peak metamorphic temperatures up to about 650°C, whereas rocks about 15 km farther southeast have only experienced 300°C. The Franz Josef Glacier flows almost parallel to this temperature gradient. The rocks are highly fractured but have uniform, steep bedding and foliation (60° to 80°) without kilometer-scale variations in strength or erodability across the catchment. The rocks also contain fossil organic carbon (*26*), which can quantify the peak metamorphic temperature conditions based on Raman spectroscopy of carbonaceous material (RSCM) (*27*). By comparing RSCM temperature data in samples collected from

[1]Institute of Earth Surface Dynamics, University of Lausanne, CH-1015 Lausanne, Switzerland. [2]Institut de Minéralogie, de Physique des Matériaux, et de Cosmochimie, Sorbonne Universités, UMR CNRS 7590, Université Pierre et Marie Curie Paris 06, Muséum National d'Histoire Naturelle, Institut de Recherche pour le Développement UMR 206, 4 place Jussieu, 75005 Paris, France. [3]Division of Geological and Planetary Science, California Institute of Technology, Pasadena, CA, USA. [4]Institute of Earth Sciences, University of Lausanne, CH-1015 Lausanne, Switzerland. [5]Division of Engineering and Applied Science, California Institute of Technology, Pasadena, CA, USA. [6]Institute of Geological and Nuclear Sciences, Private Bag 1930, Dunedin, New Zealand.
***Corresponding author. E-mail: frederic.herman@unil.ch**

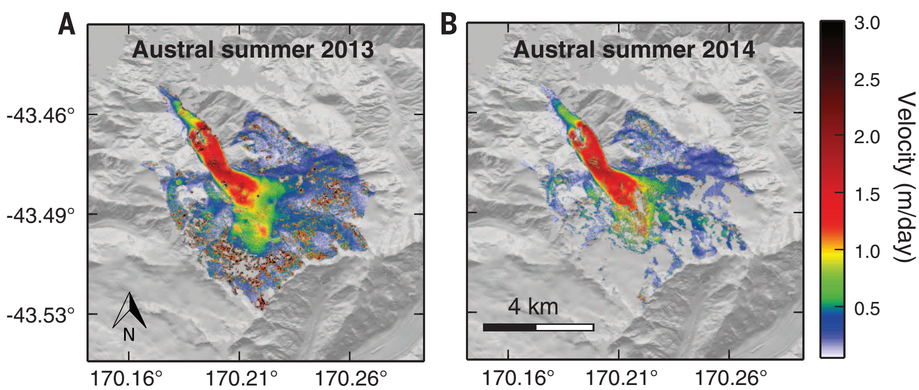

Fig. 1. Franz Josef Glacier surface velocity. The Franz Josef Glacier (Ka Roimata o Hinehukatere in Māori) is located in Westland Tai Poutini National Park on the west coast of New Zealand's South Island. (**A**) Surface velocity measured in summer 2013 (integrated over 10 days). (**B**) Surface velocity measured in summer 2014 (integrated over 12 days). The three-dimensional (3D) velocities were derived from the measurements of the 3D displacement derived from Worldview stereo images (*23*).

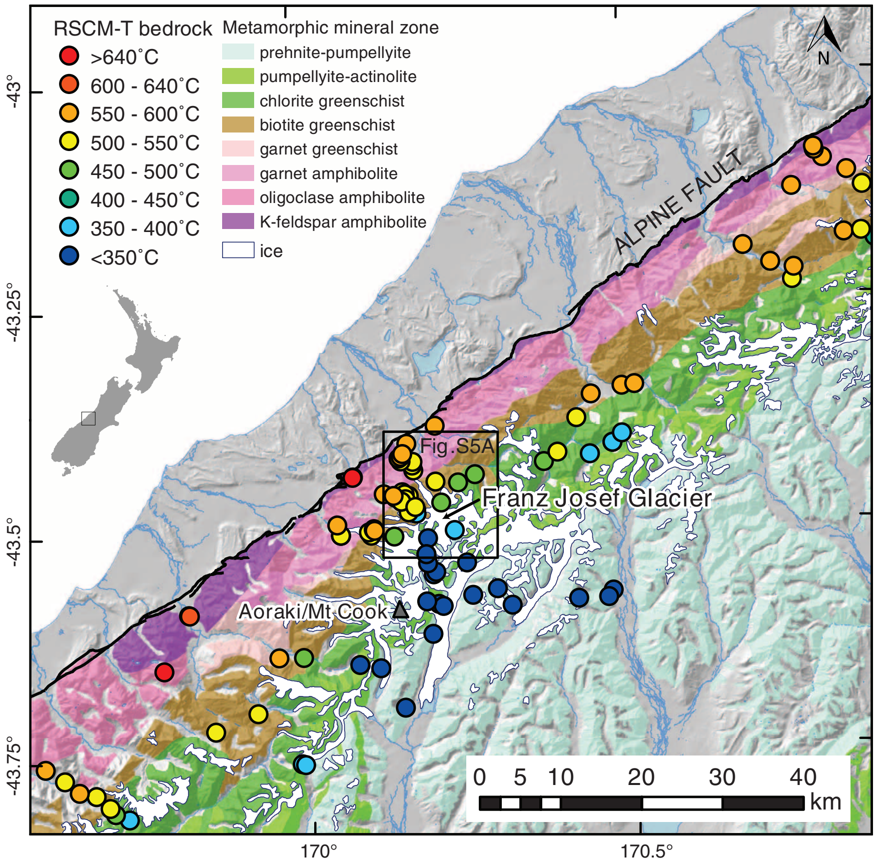

Fig. 2. Bedrock metamorphism and RSCM temperature data in the Southern Alps of New Zealand (table S2). A metamorphic map (*25*) and RSCM temperature data (*23*) are shown. Both metamorphism and RSCM temperature data show a sharp gradient in the hanging wall of the Alpine Fault. The inset is the location of the Franz Josef Glacier shown in fig. S5, which shows the bedrock temperature model used for the provenance analysis.

the glacial stream, we determined the provenance of the particulate load found in the glacial stream (*23*). We were then able to reconstruct the magnitude and patterns of erosion.

Our results show erosion patterns closely mimicking the velocity patterns over the 5-month period (fig. S2). Maximum erosion rates occurred around the steeper, faster parts of the glacier. Low erosion rates correspond either to the slowly moving accumulation area or the glacier front. Analysis of the temporal evolution of glacial erosion reveals that instantaneous erosion rates varied by several orders of magnitude over the 5-month period (from about 1 to 500 mm/year; movie S1). Erosion rates were highest in response to large rain events. During that time, water easily reached the ice/bedrock interface to induce an increase of water pressure, glacier sliding velocity, and erosion rates (*13*, *15*, *20*, *28*, *29*). The water discharge data we collected confirm a study showing that the subglacial drainage system does not evolve from a cavity-driven to a channelized system through time (*23*, *29*). These observations explain why we continuously observed such a high sensitivity to water inputs. Furthermore, the integrated erosion rates over the 5-month period compare well to rates integrated over geological time scales (*30*). This suggests the potential to extrapolate the processes driving erosion during our observations to longer time scales.

We combined the integrated erosion rates with the provenance and remote sensing data to constrain the parameters in an erosion law (Fig. 3A). We assume that the erosion rate is proportional to the sliding velocity raised to some power (i.e., $\dot{e} = K_g|u_s|^l$, where $\dot{e}$ is the erosion rate, K_g is an erodability constant, u_s is the sliding velocity, and l is an exponent). We constrained K_g and l using two independent methods. The first one is based on the nonlinear least-squares method, and the second is based on Bayesian inversion that enables us to construct the probability density function of the constrained parameters (*23*). Both approaches lead to a nonlinear relationship, with an exponent l close to 2 (Fig. 3, A, B, and D). This relationship agrees with theoretical predictions for glacial abrasion (*5*). Abrasion is proportional to the product of the viscous drag force of the ice as it moves on the bedrock and the rate at which debris contained in the ice is dragged against the bed, which both depend on the sliding velocity.

Theoretical models for abrasion and quarrying assume basal sliding to be the primary driver of erosion (*5*–*7*). Discriminating which of these two processes dominates is known to be difficult. This is in part because other variables than sliding play a role, including lithological variations or subglacial fluvial activity. One quarrying model (*7*) accounts for the effect of bedrock strength heterogeneities and variations in water pressure at the ice/bedrock interface. It predicts an erosion exponent $l < 1$ for weak bedrock strength such as that in the Southern Alps. The model also implies decreasing or relatively steady erosion rates with increasing water pressure (*7*), in contrast to our observations of a different relationship (movie S1). This relationship, along with our sliding velocity exponent of about 2, may imply an abrasion-dominated process in the Franz Josef Glacier, although quarrying is required to produce rock fragments that abrade the bedrock.

Existing field estimates in Alaska (*19*), the European Alps (*19*), and the Patagonian Andes (*18*) all suggested an exponent l of 1 and a dimensionless K_g around 10^{-4}. Most landscape evolution models use these values. We observed similar values when spatially integrating erosion rates and sliding velocities for the Franz Josef Glacier. Unfortunately, spatially integrated erosion rates and velocities (*19*, *20*) cannot rigorously constrain K_g and l independently because of the trade-off between the erosion constant K_g and the exponent l (Fig. 3B).

Our observations establish that glacial abrasion is a nonlinear function of ice-sliding velocity. Ice-sliding velocity is to a first order nonlinearly proportional to ice thickness and ice surface slope [eq. 9 in (*23*, *31*)], which are both set by the balance between the glacier mass balance and the divergence of the ice flux [eq. 8 in (*23*, *31*)]. As a result, an increase of ice flux induced by climate change, or increased surface slope, will be accommodated by faster sliding velocities in a nonlinear way. An additional nonlinearity on the sliding exponent in the erosion law (i.e., $l > 1$) thus implies a very high sensitivity of erosion rates to changes in ice flux (*23*). Therefore, fast-flowing glaciers are likely to be particularly effective at erosion, and

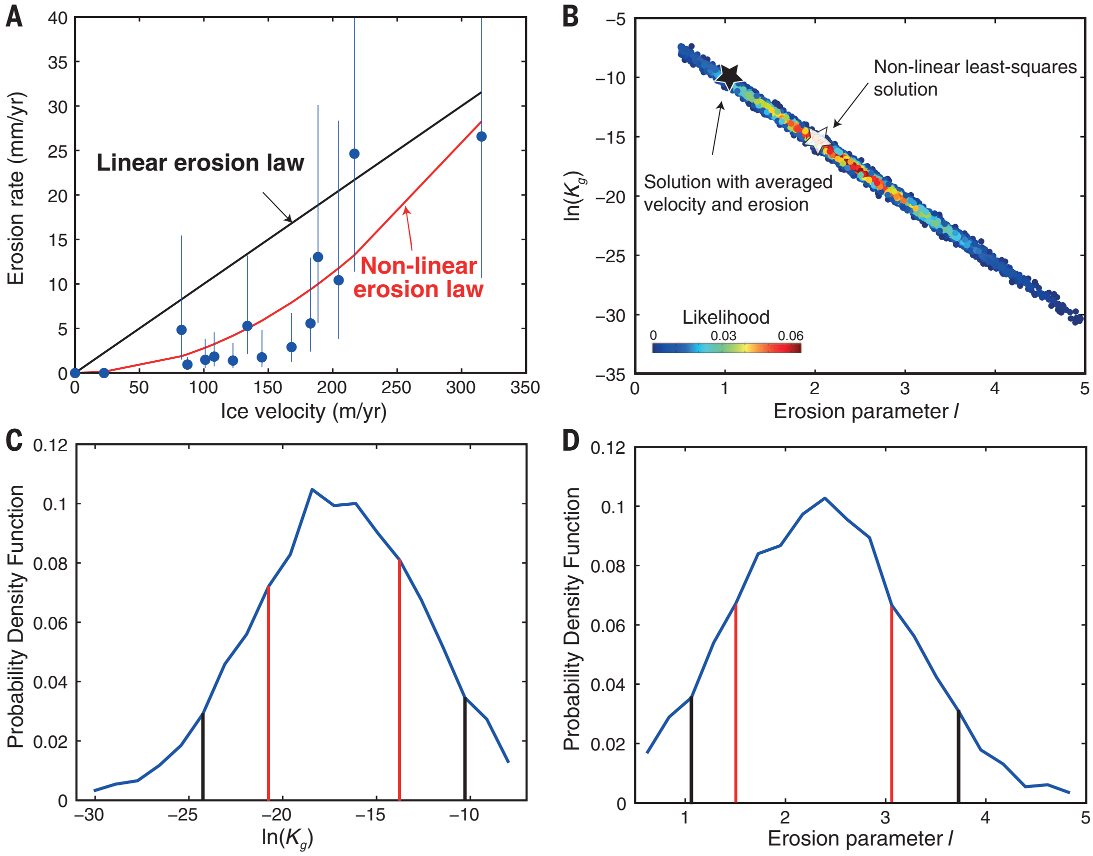

Fig. 3. Constraints on abrasion law. (**A**) Erosion rate versus sliding velocity. The blue dots represent measured velocities and integrated erosion rates using a 1-km bin size. Red and black lines correspond to the erosion rate predictions with l = 2.02 and K_g= 2.7 10^{-7} (m^{1-l}/$year^{1-l}$) and l = 1 and K_g = 10^{-4}, respectively. The magnitude of the error bars comes from the variability of erosion rates through time. (**B**) Erosion exponent l versus the natural logarithm of erosion constant K_g. Each dot represents sampling of the maximum-likelihood solution, with dots being colored according to their likelihood (from blue to red, with red being most likely) (*23*). The black star is the estimated value when integrating erosion and velocity over the entire glacier. The white star indicates values obtained with the non-linear least-squares fit (*23*). The quality of fit to data for each dot in (A) is shown in fig. S2. (**C** and **D**) Probability density functions for K_g and l, respectively (*23*). Black and red bars indicate 90 and 60% confidence intervals.

abrasion might become the dominating process over quarrying for fast-flowing glaciers over weak rocks, such as the Franz Josef Glacier.

The nonlinear glacial erosion law may explain why glacial erosion rates span several orders of magnitude, from polar dry regions to temperate alpine glaciers and from soil-mantled hillslope landscapes to steep, tectonically active mountain ranges (*4*, *17*, *18*). Atmospheric circulation controls global precipitation, with precipitation increasing from the poles to the equator. In addition, the polar jet stream and its associated westerly winds have a major influence on glacial access to precipitation as they bring moisture onto continents. Several observations suggest that they migrate toward the equator during glacial periods (*32*). These effects, combined with the nonlinear response of glacial erosion to precipitation changes, would provide an appealing explanation for why the impact of glaciation was more pronounced in mid-latitude regions with steep topography during the Quaternary (*4*).

REFERENCES AND NOTES

1. P. Molnar, P. England, *Nature* **346**, 29–34 (1990).
2. J. H. Tomkin, G. H. Roe, *Earth Planet. Sci. Lett.* **262**, 385–397 (2007).
3. J. Braun, D. Zwartz, J. H. Tomkin, *Ann. Glaciol.* **28**, 282–290 (1999).
4. F. Herman *et al*., *Nature* **504**, 423–426 (2013).
5. B. Hallet, *J. Glaciol.* **17**, 209–222 (1979).
6. B. Hallet, *Ann. Glaciol.* **22**, 1–8 (1996).
7. N. R. Iverson, *Geology* **40**, 679–682 (2012).
8. J. Harbor, B. Hallet, C. F. Raymond, *Nature* **333**, 347–349 (1988).
9. K. R. MacGregor, R. S. Anderson, S. P. Anderson, E. D. Waddington, *Geology* **28**, 1031–1034 (2000).
10. D. L. Egholm, S. B. Nielsen, V. K. Pedersen, J. E. Lesemann, *Nature* **460**, 884–887 (2009).
11. K. R. MacGregor, R. S. Anderson, E. D. Waddington, *Geomorphology* **103**, 189–204 (2009).
12. M. A. Kessler, R. S. Anderson, J. P. Briner, *Nat. Geosci.* **1**, 365–369 (2008).
13. F. Herman, F. Beaud, J.-D. Champagnac, J.-M. Lemieux, P. Sternai, *Earth Planet. Sci. Lett.* **310**, 498–508 (2011).
14. T. T. Creyts, G. K. C. Clarke, M. Church, *J. Geophys. Res.* **118**, 423–446 (2013).
15. F. Beaud, G. E. Flowers, S. Pimentel, *Geomorphology* **219**, 176–191 (2014).
16. R. B. Alley, D. E. Lawson, G. J. Larson, E. B. Evenson, G. S. Baker, *Nature* **424**, 758–760 (2003).
17. B. Hallet, L. Hunter, J. Bogen, *Global Planet. Change* **12**, 213–235 (1996).
18. M. N. Koppes, D. R. Montgomery, *Nat. Geosci.* **2**, 644–647 (2009).
19. N. F. Humphrey, C. F. Raymond, *J. Glaciol.* **40**, 539–552 (1994).
20. C. A. Riihimaki, K. R. MacGregor, R. S. Anderson, S. P. Anderson, M. G. Loso, *J. Geophys. Res.* **110**, F03003 (2005).
21. D. A. Swift, P. W. Nienow, T. B. Hoey, *Earth Surf. Process. Landf.* **30**, 867–883 (2005).
22. J. Oerlemans, *Arct. Alp. Res.* **29**, 233–239 (1997).
23. Materials and methods are available as supplementary materials on *Science* Online.
24. B. Anderson, W. Lawson, I. Owens, B. Goodsell, *J. Glaciol.* **52**, 597–607 (2006).
25. S. C. Cox, D. J. A. Barrell, *Geology of the Aoraki Area* (1:250,000 geological map 15, Institute of Geological and Nuclear Sciences, GNS Science, Lower Hutt, New Zealand, 2007), 71 pp. + 1 folded map.
26. R. G. Hilton, A. Galy, N. Hovius, *Global Biogeochem. Cycles* **22**, GB1017 (2008).
27. O. Beyssac, B. Goffé, C. Chopin, J. N. Rouzaud, *J. Metamorph. Geol.* **20**, 859–871 (2002).
28. R. L. Hooke, *Geol. Soc. Am. Bull.* **103**, 1104–1108 (1991).
29. B. Anderson *et al*., *Arct. Antarct. Alp. Res.* **46**, 919–932 (2014).
30. T. A. Little, S. Cox, J. K. Vry, G. Batt, *Geol. Soc. Am. Bull.* **117**, 707 (2005).
31. K. M. Cuffey, W. S. B. Paterson, *The Physics of Glaciers* (Butterworth-Heinemann/Elsevier, Oxford, ed. 4, 2010).
32. G. H. Denton *et al*., *Science* **328**, 1652–1656 (2010).

ACKNOWLEDGMENTS

The authors thank B. Anderson for field support. F.H., M.B., and S.L thank the Fonds d'Investissement from the Faculty of Geosciences and Environnement at the University of Lausanne. F.H. was funded by Swiss National Science Foundation grant PP00P2_138956. S.L, J.Y.L., and J.-P.A. were funded by the Gordon and Betty Moore Foundation through grant GBM 2808 and NSF Earth Sciences grant 1348704. O.B. was funded by the City of Paris (Emergence Program), Institut National des Sciences de l'Univers, and Sorbonne Universités (Per-SU program). Three anonymous reviewers are thanked for their constructive reviews. K. Cuffey is thanked for his feedback. Data are available in the supplementary materials.

SUPPLEMENTARY MATERIALS

www.sciencemag.org/content/350/6257/193/suppl/DC1
Materials and Methods
Figs. S1 to S10
Tables S1 and S2
References (*33*–*53*)
Movies S1 and S2

31 March 2015; accepted 3 September 2015
10.1126/science.aab2386

Erosion by an Alpine glacier
Frédéric Herman *et al.*
Science **350**, 193 (2015);
DOI: 10.1126/science.aab2386